Phase Transformation of Nanosized ZrO2 Upon Thermal Annealing and Intense Radiation

ARTICLE *in* THE JOURNAL OF PHYSICAL CHEMISTRY C · MARCH 2011

Impact Factor: 4.77 · DOI: 10.1021/jp109558s

THE JOURNAL OF PHYSICAL CHEMISTRY C

ARTICLE

pubs.acs.org/JPCC

Phase Transformation of Nanosized ZrO_2 upon Thermal Annealing and Intense Radiation

Fengyuan Lu,[†] Jiaming Zhang,[‡] Mengbing Huang,[§] Fereydoon Namavar,[⊥] Rodney C. Ewing,[‡] and Jie Lian*[,†]

[†]Department of Mechanical, Aerospace & Nuclear Engineering, Rensselaer Polytechnic Institute, Troy, New York 12180, United States

[‡]Departments of Geological Sciences and Materials Science & Engineering, University of Michigan, Ann Arbor, Michigan 48109-1005, United States

[§]College of Nanoscale Science and Engineering, The University at Albany-The State University of New York, 255 Fuller Road, Albany, New York 12203, United States

[⊥]University of Nebraska Medical Center, Omaha, Nebraska 68198, United States

ABSTRACT: The phase stability and microstructure evolution of zirconia nanofilms on Si substrates prepared by ion beam assisted deposition (IBAD) upon thermal annealing and intensive radiation have been studied by in situ transmission electron microscopy (TEM), ex situ X-ray diffraction, and Raman spectroscopy. For as-prepared amorphous-dominant ZrO_2 thin films, a phase transformation sequence of amorphous-to-tetragonal and tetragonal-to-monoclinic has been identified upon increasing annealing temperature from 500, 850, to 1000 °C. This phase transformation sequence varying with annealing temperature is accompanied by concomitant grain growth from ~5 to ~50 nm, consistent with the grain-size-controlled phase stability as a result of total energy crossover among different zirconia polymorphs. Upon ion bombardments of 350 KeV O^+ and 1 MeV Kr^{2+} at room temperature, a monoclinic-to-tetragonal phase transformation was observed in the monoclinic-dominant ZrO_2. This monoclinic-to-tetragonal phase transformation may be attributed to the oxygen vacancy accumulation in ZrO_2 upon irradiation. Furthermore, both 1 MeV Kr^{2+} and 350 KeV O^+ bombardments on the amorphous-dominant ZrO_2 lead to an amorphous-to-tetragonal phase transformation as a result of radiation-induced recrystallization process. Thermodynamically metastable tetragonal ZrO_2 phase can be stabilized at room temperature under intensive radiation by relatively low-energy ion bombardments. These results suggest a method of combining both thermal annealing and ion beam technique for controlling ZrO_2 phase stability and thus tailoring materials properties for many engineering applications including actinide host matrix for advanced nuclear energy systems.

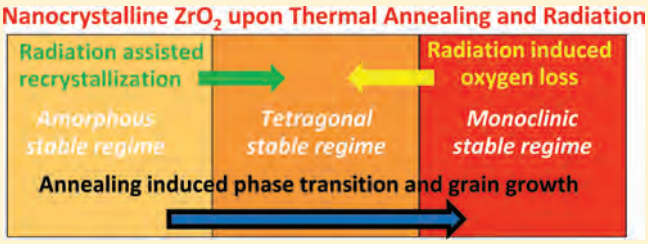

1. INTRODUCTION

Zirconia (ZrO_2) displays attractive physical, mechanical, and electrical properties and high chemical durability and thus has wide technological applications, and so forth, thermal barrier or wear resistant coatings, catalysts, gas sensors, electrolytes in solid oxide fuel cells, and gate dielectric in microelectronics. Zirconia polymorphs also demonstrate excellent radiation tolerance and are important engineering materials for nuclear applications.[1,2] Specifically, to reduce the total inventory of radiotoxic plutonium and other minor actinides and effectively utilize nuclear resources, ZrO_2 has been suggested as a promising host matrix to incorporate actinides, such that they can be used as inert fuel matrix in nuclear reactors or waste forms in geological repository environments.[3−5] However, ZrO_2 has polymorphs of cubic, tetragonal, monoclinic, and amorphous structures, and phase transformation among them can be induced by high temperature,[6,7] high pressure,[8,9] or radiation,[10,11] greatly affecting the physical and mechanical properties of ZrO_2 utilized as fuel or hosting matrix for nuclear applications. The phase transformations among zirconia polymorphs are complex, varying with the crystal size, temperature, and irradiation conditions. On the basis of previous studies, thermal annealing can induce crystalline-to-crystalline phase transformation in ZrO_2,[6,7] and ion irradiation can induce either crystalline-to-crystalline[11] or crystalline-to-amorphous[12] or amorphous-to-crystalline[13] phase transformations. Therefore, it is critically important to investigate the phase stability of ZrO_2 and the underlying physics governing the phase transformation processes upon thermal annealing and intensive radiation for various engineering applications, for example, designing ZrO_2-based host matrix for actinide incorporation with enhanced materials performance for advanced nuclear energy systems.

Furthermore, nanocrystalline zirconia has its unique mechanical, thermal, and electrical properties as compared to its bulk counterparts, and the phase stability of nanosized zirconia can be significantly affected by their grain size. It is of particular importance to control the phase stability of different polymorphs (amorphous, cubic, tetragonal, and monoclinic phases) at

Received: October 5, 2010
Revised: February 5, 2011
Published: March 25, 2011

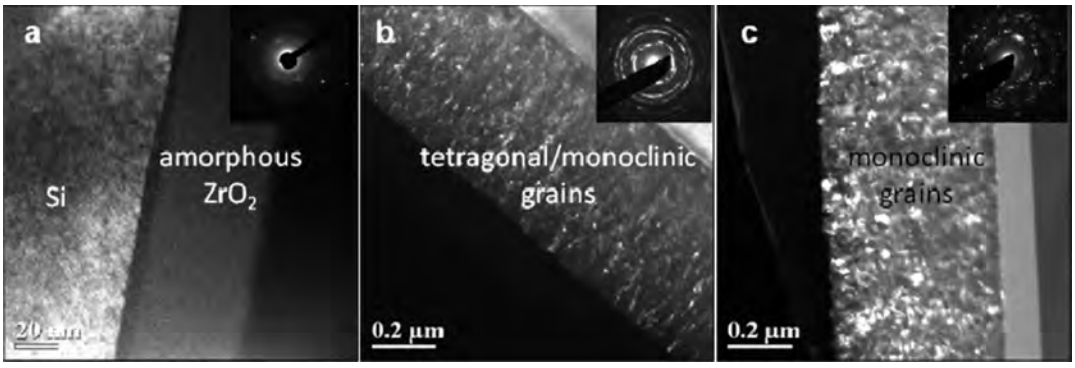

Figure 1. TEM dark field images of (a) originally unannealed ZrO_2 sample, and the inserted SAED pattern of the ZrO_2 thin film confirms predominant amorphous structure; (b) 500 °C annealed ZrO_2 sample with the formation of nanocrystalline grains and the inserted SAED pattern showing the existence of tetragonal and monoclinic phase; (c) 1000 °C annealed ZrO_2 sample, the average grain-size has increased to 40−50 nm, and the phase is shown by the inserted SAED as dominantly monoclinic.

different size regimes. In this study, the phase stability of nanosized ZrO_2 has been studied by thermal annealing of ZrO_2 at different temperatures, and ZrO_2 phase transformation upon intensive radiations has been investigated by energetic ion beam irradiations. A sequence of amorphous-to-tetragonal and tetragonal-to-monoclinic phase transformation induced by thermal annealing has been observed, and ZrO_2 grain growth has been found directly correlated to the annealing-induced phase transformations. In contrast, energetic ion beams can induce a monoclinic-to-tetragonal phase transformation, which will suppress the annealing effect. An amorphous-to-tetragonal phase transformation upon ion irradiation is also achieved by ion irradiation. These results highlight important implications of using both thermal annealing and radiation to control the phase stability and thus tailor the physical and mechanical properties of zirconia for a wide range of engineering applications.

2. EXPERIMENTS

The amorphous ZrO_2 thin film used in this study was prepared by ion beam assisted deposition (IBAD) at the Nanotechnology Laboratory of the University of Nebraska Medical Center. Monoclinic ZrO_2 of 99.7% purity was used as the source, evaporated by a 500 eV ion beam of mixed Ar, O, and N ions, and deposited on a silicon substrate in an ultrahigh vacuum environment at a base pressure of 2×10^{-7} Torr.[14] Prior to ZrO_2 deposition, substrates were ion beam cleaned by a high-intensity argon beam for about 15 min. Typical nanocrystalline zirconia oxide upon IBAD synthesis was studied by secondary ion mass spectrometry (SIMS) measurements, and no other impurities could be observed except argon or nitrogen used as ions for bombardment. Typically, the concentration of these elements was less than a fraction of 1%. During the deposition of ZrO_2, the temperature of the substrate holder was controlled from room temperature to around 100 °C as determined by a thermocouple. Microstructures of the thin films were characterized by cross-sectional TEM examinations using a JEOL-2010F TEM. The Raman spectra were measured using a Jobin-Yvon HR300 Raman spectrometer equipped with a 632.8 nm red laser source, and the X-ray diffraction patterns were collected by a PANalytical X'pert Pro X-ray diffractometer.

The as-prepared amorphous ZrO_2 thin film samples were thermally annealed in an ultra clean alumina tube furnace in air at 500 °C for 20 days, and 850 and 1000 °C for 1 h, respectively, and the phase compositions and microstructural evolution of the thin films were characterized by ex situ TEM, X-ray diffraction (XRD), and Raman spectroscopy. For investigating the phase stability under intensive radiation conditions, both 350 KeV O^+ and 1 MeV Kr^{2+} ion beams were used to irradiate the samples. The 350 KeV O^+ irradiation was conducted at the Ion Beam Laboratory of the State University of New York at Albany on the as-prepared ZrO_2 and the ZrO_2 samples annealed at 500 °C, 850 and 1000 °C. Ex situ X-ray diffraction and Raman spectroscopy were done on the irradiated samples to determine the phases present and detect any structural transformation upon oxygen irradiation. The 1 MeV Kr^{2+} irradiation was performed on the 1000 °C annealed ZrO_2 at the IVEM-tandem facility at Argonne National Laboratory, where the ion accelerator is connected with a Hitachi-9000 TEM. The ZrO_2 phase evolution upon 1 MeV Kr^{2+} irradiation was monitored in situ by TEM imaging and selected area electron diffraction (SAED) techniques.

3. RESULTS AND DISCUSSION

3.1. Thermal Annealing-Induced Phase Transformation and Grain Growth. Part a of Figure 1 shows a dark field TEM image of the original thin film deposited on Si substrates. The amorphous rings dominating the SAED pattern of the ZrO_2 thin film (insert in part a of Figure 1) suggest an amorphous-dominant feature in the original thin films, consistent with the lack of contrast in the dark field TEM image (part a of Figure 1) due to poor crystallinity in the as-deposited films. High-resolution TEM images of the original films indicate that small amounts of nanocrystalline grains in the cubic or tetragonal structure exist with a mean size of ~5 nm. Additionally, ex situ XRD pattern (as shown in Figure 2) and Raman spectrum (Figure 3) of the original thin film do not contain characteristic peaks from crystalline ZrO_2, confirming that the sample is dominated by amorphous phase.

Parts b and c of Figure 1 show cross-sectional TEM images of the ZrO_2 films annealed at 500 and 1000 °C for 20 days and 1 h, respectively. Upon annealing at 500 °C, considerable amounts of nanocrystalline grains formed from the amorphous ZrO_2, as evidenced by the bright contrast in dark field TEM images. A mixture of monoclinic and tetragonal polymorphs was identified based on the corresponding SAED pattern (insert in part b of Figure 1). By increasing the annealing temperature to 1000 °C,

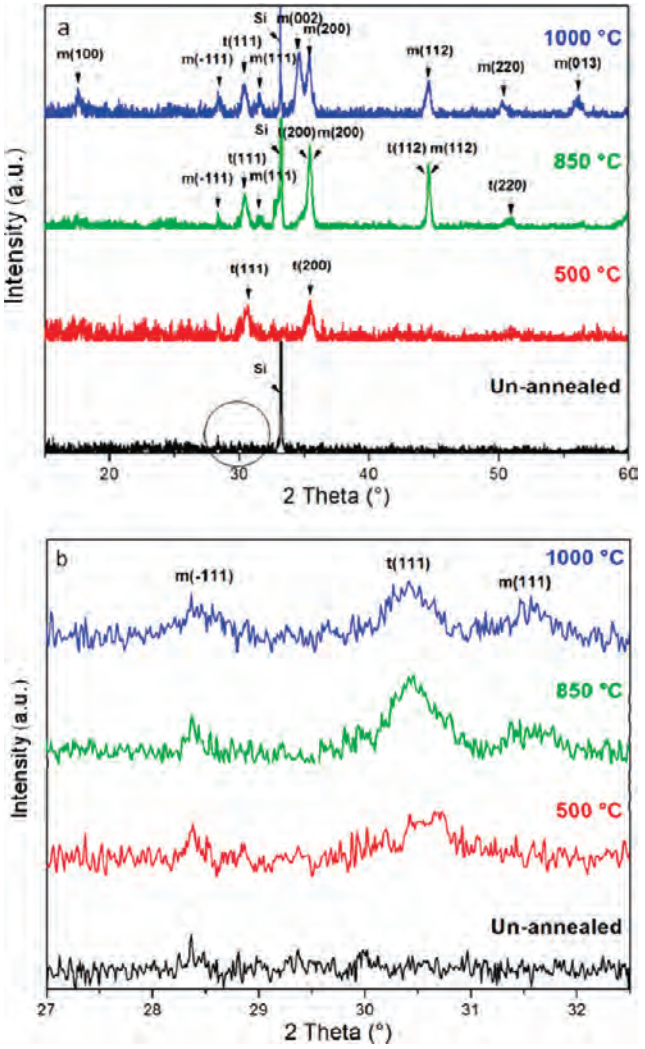

Figure 2. (a) XRD patterns of the unannealed, 500 °C annealed, 850 °C annealed and 1000 °C annealed ZrO_2 thin films, where t and m denote tetragonal and monoclinic phases, respectively. The signal of silicon substrates was also observed as denoted by Si. Note that the overlapping of XRD peaks occurs between tetragonal and monoclinic peaks. (b) Close-up XRD patterns of zirconia films annealed at different temperatures within the 2θ range of 27° to 32.5° to differentiate the characteristic peaks of tetragonal phase from monoclinic phase.

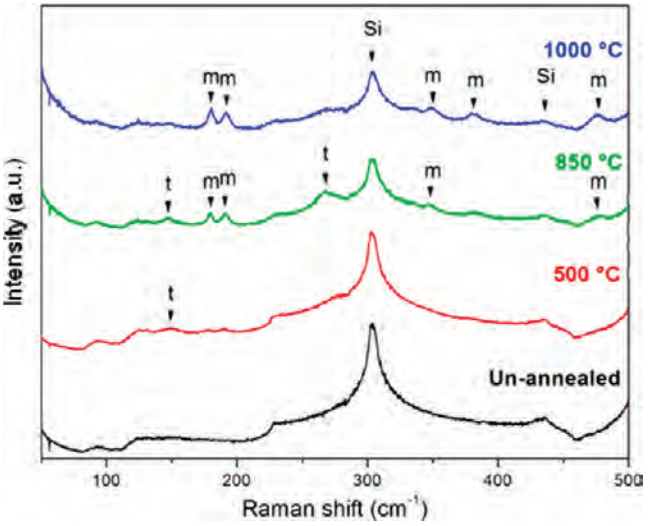

Figure 3. Raman spectra of ZrO_2 samples with different thermal treatments: unannealed, 500 °C annealed, 850 °C annealed, and 1000 °C annealed, where t and m denote characteristic peaks from tetragonal and monoclinic phases, respectively. The Raman signals from Si substrates were also observed.

ZrO_2 was transformed into a monoclinic-dominant phase as indicated by the inserted SAED pattern (part c of Figure 1).

Ex situ XRD characterizations have been conducted to confirm the ZrO_2 phase composition occurring after thermal annealing at different temperatures, as shown in Figure 2. To avoid the ZrO_2 monoclinic and tetragonal overlap in the XRD patterns, an expanded XRD pattern in the 2θ range of 27°−32.5° is included (part b of Figure 2), where monoclinic and tetragonal characteristic peaks can be clearly distinguished. The featureless pattern of the originally unannealed ZrO_2 thin film verifies the amorphous dominance in the sample. Upon 500 °C annealing for 20 days, two peaks from tetragonal (111) and (200) planes appear, indicating the formation of a dominantly tetragonal phase. At 850 °C, the XRD pattern shows both significant ZrO_2 monoclinic and tetragonal characteristic peaks, which is a result of a mixture of tetragonal and monoclinic phases in the ZrO_2 thin film. As the annealing temperature is increased to 1000 °C, the ZrO_2 tetragonal peaks are reduced remarkably, while the monoclinic peaks become stronger, consistent with the SAED result of part c of Figure 1, which shows a dominantly monoclinic phase.

Raman spectroscopy is a sensitive tool for detecting the corresponding bonding changes in ZrO_2 upon annealing, whose results are shown in Figure 3. Because of the XRD peak overlap, it may be difficult to distinguish the ZrO_2 tetragonal phase from the cubic phase solely by XRD.[15,16] Therefore, the Raman spectroscopy results are combined with XRD and SAED to further identify tetragonal ZrO_2. Similar methods have also been applied by many other researchers for determining the ZrO_2 tetragonal phase.[17−20] In the unannealed sample, except for the two peaks at ∼305 and ∼435 cm^{-1} from the silicon substrate, the Raman spectrum shows a mostly amorphous phase without significant ZrO_2 characteristic bonding peaks. As the annealing temperature is increased to 500 °C, tetragonal phase becomes dominant as indicated by the emerging tetragonal ZrO_2 B_{1g} vibration mode at ∼150 cm^{-1}, with a minor fraction of monoclinic phase indicated by the weak monoclinic ZrO_2 $A_g + B_g$ and A_g vibration modes at ∼177 cm^{-1} and ∼186 cm^{-1}, respectively.[21,22] By further increasing the annealing temperature to 850 °C, Raman scattering from both tetragonal phase and monoclinic phase becomes prominent. When the annealing temperature reaches 1000 °C, Raman signals from tetragonal phase almost disappear, and the vibration modes from monoclinic phase become dominant in the Raman spectrum, suggesting that the tetragonal phase largely transforms to a monoclinic phase upon thermal annealing, consistent with the TEM and XRD results (Figures 1 and 2).

On the basis of the combination of the results of TEM, XRD, and Raman spectroscopy, the phase evolution for nanosized ZrO_2 upon thermal annealing follows a transformation sequence: (1) an amorphous-dominant phase transforms to a tetragonal phase at an annealing temperature slightly below 500 °C; (2) in the annealing temperature range of 500−850 °C, a tetragonal-to-monoclinic phase transformation begins, leading to a coexistence

dx.doi.org/10.1021/jp109558s |J. Phys. Chem. C 2011, 115, 7193–7201

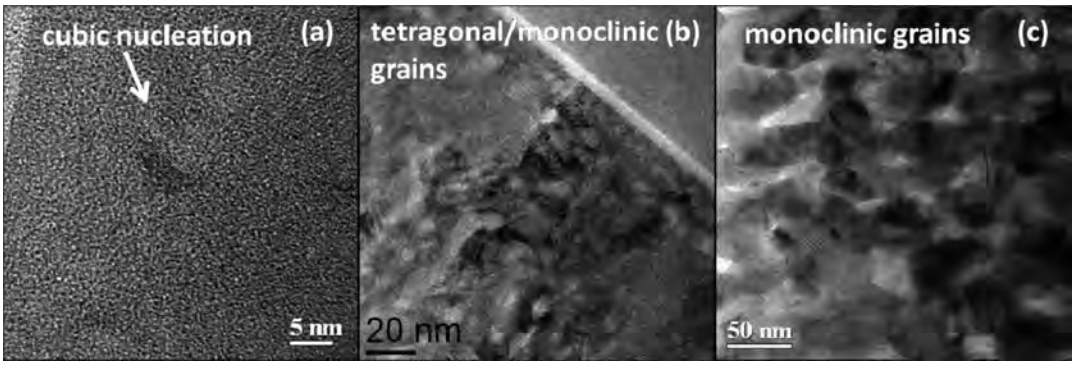

Figure 4. (a) High-resolution TEM image showing that ~5 nm nanocrystalline cubic/tetragonal grains sparsely distributed within the amorphous matrix, (b) bright field TEM image of 500 °C annealed ZrO_2 showing tetragonal or monoclinic phases with the size of 10−20 nm, (c) bright field TEM image of the 1000 °C annealed ZrO_2 showing dominantly monoclinic grains with average sizes of 40−50 nm.

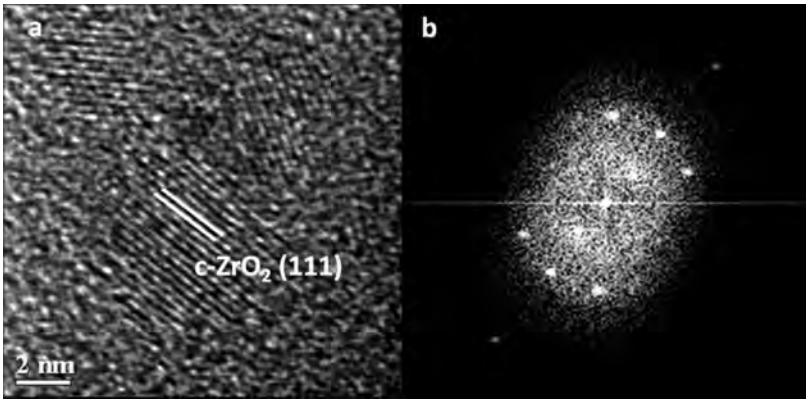

Figure 5. (a) HRTEM image of the nanocrystalline grains distributed in the unannealed amorphous-dominant sample, (b) inverse FFT result of (a) indicates a cubic/tetragonal structure.

of tetragonal and monoclinic phases; and (3) the phase mixture is further transformed to a monoclinic-dominant phase upon 1000 °C annealing. In brief, the thermal annealing induced phase transformation is a two-step sequence consisting of amorphous-to-tetragonal and tetragonal-to-monoclinic transitions.

Accompanying with the two-step annealing induced ZrO_2 phase transformation, a grain growth from the nanocrystalline grains dispersed in the original amorphous-dominant ZrO_2 thin film can be observed. The grain growth can be clearly seen by the larger areas showing bright contrast in the dark field images and discrete diffraction ring patterns for the annealed samples (Figure 1). To investigate the relation between phase transformation and grain growth, detailed high-resolution TEM imaging and bright field imaging were performed showing the morphology and structures of these samples. In part a of Figure 4, in the amorphous-dominant unannealed ZrO_2 thin film, nanocrystalline grains with ~5 nm mean diameters can be found sparsely distributed within the amorphous matrix. A high-resolution transmission electron microscopy (HRTEM) image of one such nanocrystalline grain is shown in part a of Figure 5, and the inverse fast Fourier transformed (FFT) image (part b of Figure 5) of the 2D lattice image indicates that the nanocrystalline grain is either cubic or tetragonal ZrO_2. Because of the low concentration and small volumes of the cubic/tetragonal nanocrystalline residues, it is difficult to characterize them by SAED or Raman spectroscopy. Such cubic/tetragonal residues can behave as preferential sites for grain growth in the amorphous-dominant ZrO_2. By annealing at 500 °C, significant crystallization of amorphous ZrO_2 can be clearly seen as nanocrystalline grains occupying the entire area with a mean grain-size in the range of 10−20 nm (part b of Figure 4). These nanocrystalline grains exist in both tetragonal and monoclinic phases, and further increase in the annealing temperature to 1000 °C leads to the grain growth of nanocrystallites to larger grains with a mean size of 40−50 nm, as shown in part c of Figure 4.

The ZrO_2 phase transformation sequence upon annealing is closely related to grain growth, consistent with the grain-size-controlled phase stability for nanostructured zirconia. Specifically, the variation in the total energy of different ZrO_2 polymorphs in different size regimes may drive the phase transformation during thermal annealing for nanosized ZrO_2. Clearfield reported a similar phase transformation sequence of amorphous → tetragonal + monoclinic → monoclinic by heating amorphous precipitate of hydrous ZrO_2, but little information about crystallite size was mentioned.[23] Garvie suggested that such occurrence of tetragonal phase can be found at room temperature only below a critical crystallite size of ~30 nm.[24] The change of grain size and consequent surface area of nanostructured materials significantly affects their phase stability, and an energy crossover has been reported for nanosized ZrO_2, in which the thermodynamically metastable phase in the bulk is energetically favorable as the grain size decreases

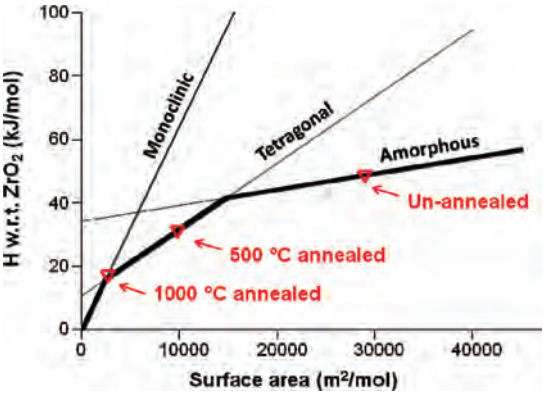

Figure 6. Comparison of grain-size (converted to surface area) and thermal annealing controlled phase stability for nanosized zirconia. The energy crossovers of nanocrystalline ZrO_2 as a function of grain size was originally reported in ref 16.

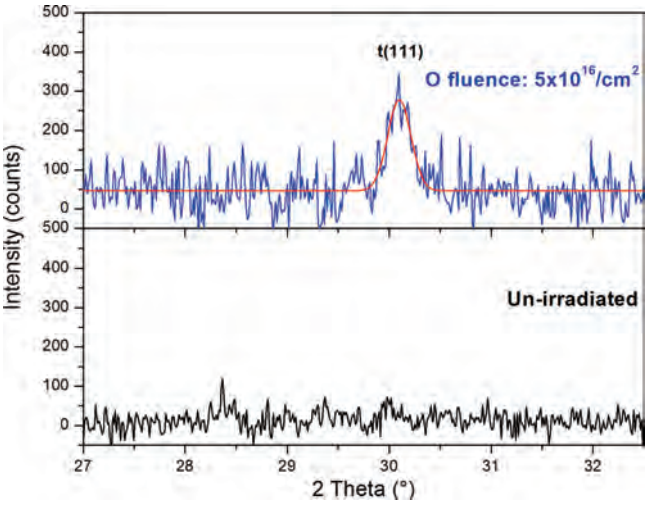

Figure 7. XRD results of ZrO_2 thin films irradiated with 350 keV O^+: unirradiated amorphous-dominant ZrO_2; ZrO_2 irradiated with 5×10^{16}/cm^2 O^+ fluence (~3.3 dpa).

below a critical value. Pitcher et al. reported that at larger size regimes, monoclinic ZrO_2 has the lowest total energy; as the size decreases into nanosized regimes, for example, below 30 nm, the total energy of tetragonal ZrO_2 becomes lower than that of monoclinic and amorphous ZrO_2, leading to the stabilization of tetragonal phase; with the grain size further decreasing below ~2−3 nm, amorphous ZrO_2 will be the most energetically stable.[25] Such correlation between grain size and phase in ZrO_2 thin films has also been reported by Namavar et al., who observed grain coalescence and a cubic-to-monoclinic phase transformation in thermally annealed nanocrystalline cubic ZrO_2 thin films.[26]

On the basis of our results of phase transformation and accompanying grain growth observed for nanosized zirconia upon thermal annealing, a close correlation between temperature and grain size in controlling the phase stability of zirconia polymorph can be identified (Figure 6). When annealed at 500 °C, the originally amorphous-dominant ZrO_2 grows to nanocrystalline grains of 10−20 nm in size, within the stable regime of the tetragonal phase. Thus, upon grain growth process,

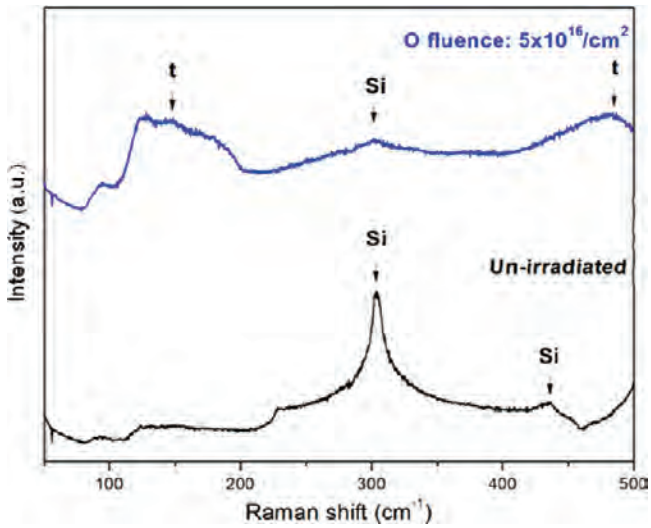

Figure 8. Raman spectra of unirradiated amorphous-dominate ZrO_2 thin films and after 350 keV O^+ irradiation at a fluence of 5×10^{16}/cm^2 (~3.3 dpa).

ZrO_2 is driven thermodynamically into a tetragonal phase stable regime, leading to the amorphous to tetragonal phase transformation. As the temperature increases to 1000 °C, the grains grow to 40−50 nm in which monoclinic phase is energetically more stable as compared with tetragonal phase, resulting in a tetragonal-to-monoclinic phase transformation. Such a correlation between grain size and stable phase in our experiments is consistent with that reported by Pitcher et al.[25] These experimental results highlight important implications for materials modification and phase transformation by thermal annealing or microstructural manipulation through energetic controls.

3.2. Microstructural Evolution and Phase Stability upon Intensive Radiation. The response of bulk zirconia with different polymorphs has been extensively studied as a result of the importance of zirconia utilized as engineering materials for nuclear applications. Particularly, bulk zirconia polymorphs show extremely high radiation tolerance, and no amorphization can be induced up to a dose of 680 displacements per atom (dpa) under 340 KeV Xe irradiation.[11] Instead of amorphization, a phase transformation from monoclinic to tetragonal or cubic phase zirconia was observed upon low-energy ion bombardments. Furthermore, such a monoclinic-to-tetragonal phase transformation can be induced by ionizing radiation using swift heavy ions above a threshold electronic energy loss (~12 keV/nm).[27] In addition, we previously reported that an amorphous matrix can transform to a tetragonal phase when irradiated by 1 MeV Kr^{2+} at room temperature as a result of a radiation-induced recrystallization process.[13] In this study, we have investigated the phase stability and microstructural evolution of nanosized zirconia upon intensive radiations simulated by energetic ion beam bombardments, and compared the radiation response to their bulk counterparts. Our data indicate that tetragonal phase can form from both amorphous and monoclinic dominant phases upon ion bombardments of 350 keV O^+ or 1 MeV Kr^{2+} for nanosized zirconia.

Ex situ XRD results of the originally amorphous-dominant ZrO_2 before and after 350 keV O^+ ion irradiation are shown in Figure 7. The tetragonal (111) diffraction peak emerged in the

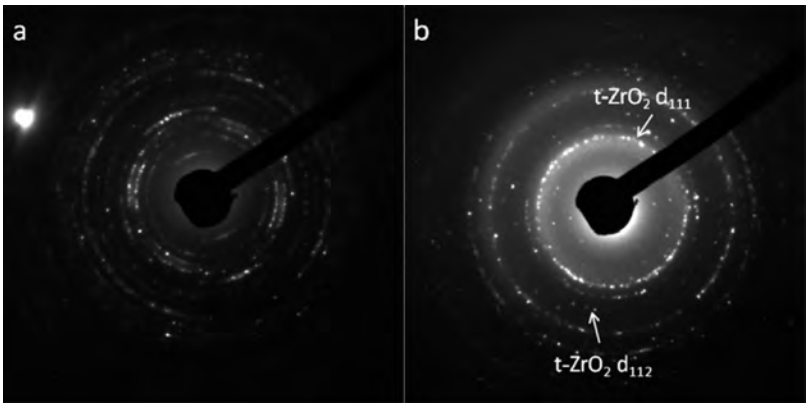

Figure 9. (a) SAED pattern of 1000 °C annealed ZrO_2 before irradiation shows monoclinic structure, (b) SAED pattern of °C annealed ZrO_2 after 1 MeV Kr^{2+} irradiation at a fluence of 3.5×10^{15} /cm^2 (~3.2 dpa) shows the existence of tetragonal phase.

sample bombarded with 5×10^{16}/cm^2 oxygen, evidencing an amorphous-to-tetragonal phase transformation. Ex situ Raman spectra in Figure 8 provide additional proof for the tetragonal phase formation. Upon oxygen irradiation, significant tetragonal ZrO_2 Raman characteristic peaks appear at 150 and 470 cm^{-1}, corresponding to vibration mode B_{1g} and A_g respectively from the largely featureless spectrum of the unannealed amorphous ZrO_2. It is noted that the Raman peaks from the Si substrate decrease significantly upon 350 keV oxygen implantations, suggesting that significant radiation damage occurred in the Si substrate. This is consistent with SRIM-08 calculations, in which almost all oxygen ions penetrated through the 100 nm ZrO_2 thin film and were implanted into the underlying Si substrate for 350 KeV O^+. The effect of oxygen implantation within zirconia nanofilms on the phase transformation of zirconia is negligible.

Interestingly, while amorphous-to-tetragonal phase transformation can be induced by ion bombardments, the monoclinic-to-tetragonal phase transformation is also achievable in nanosized zirconia. The 1000 °C annealed monoclinic-dominant ZrO_2 thin film was irradiated with 1 MeV Kr^{2+} and observed in situ with a Hitachi-9000 TEM at Argonne National Laboratory. SAED was used to determine the ZrO_2 phase during Kr^{2+} irradiation. As shown in Figure 9, electron diffraction rings from the monoclinic phase gradually fade with increasing Kr^{2+} fluence, and new diffraction rings corresponding to tetragonal (111) and (112) crystal planes emerge at a fluence of 3.5×10^{15} ions/cm^2. No significant change in average grain size after irradiation has been observed, which suggests that grain size does not have a significant effect on the radiation-induced phase transformation processes. The monoclinic-to-tetragonal phase transition observed in nanosized zirconia (50 nm) in this study is similar to ion irradiation induced monoclinic-to-tetragonal phase transformation of bulk samples under *in situ* TEM observations in previous studies.[13,28]

The displacement damage induced monoclinic-to-tetragonal phase transformation can also be induced by 350 keV O^+ irradiation, as evidenced by both XRD and Raman spectroscopy results. The XRD results in Figure 10 show the monoclinic diffraction peaks have been largely suppressed by intensive oxygen irradiation at a fluence of 5×10^{16}/cm^2; whereas the tetragonal (111) characteristic peak remains strong, suggesting that the tetragonal phase gradually dominates. The Raman spectra shown in Figure 11 also reveal that the monoclinic characteristic peaks are mostly eliminated upon 5×10^{16}/cm^2 oxygen fluence, and tetragonal characteristic peaks at ~150 cm^{-1} (B_{1g} vibration mode) and ~470 cm^{-1} (A_g vibration mode) emerge, indicating a monoclinic-to-tetragonal phase transformation. Again, the Raman signal from Si substrate decreases dramatically, suggesting significant damage in the substrate upon energetic oxygen irradiation penetrated through zirconia nanolayers.

To understand the mechanisms controlling the phase stability and structural transformation for nanosized zirconia at different radiation conditions, we performed full cascade calculations using SRIM-2008. The calculated doses for 1 MeV Kr^{2+} irradiation at a fluence of 3×10^{15} ions/cm^2 and 350 keV O^+ irradiation at a fluence of 5×10^{16} ions/cm^2 are ~3.2 and 3.3 dpa, respectively. The average electronic energy losses for 350 keV O^+ and 1 MeV Kr^{2+} in nanosized zirconia with the film thickness of 100 nm are 0.77 KeV/nm and 0.96 keV/nm, respectively. The electronic energy loss is much smaller than the threshold value (12 keV/nm) required for the monoclinic-to-tetragonal phase transformation in bulk materials upon swift heavy ion irradiation.[27] This comparison suggests that the thermal spike mechanism is not responsible for the monoclinic-to-tetragonal transformation observed in nanosized zirconia upon low-energy bombardments.

The amorphous-to-tetragonal phase transformation in nanosized zirconia might be induced by ionizing radiation-enhanced recrystallization processes. Similar to thermal annealing, the residual tetragonal/cubic crystallites may provide preferential sites for tetragonal phase grain growth. Under highly nonequilibrium conditions, for example, intense radiation, the amorphous phase can transform to the more energetically favorable tetragonal phase if the energetic beam bombardment provides enough energy to overcome the energy barrier among two phases. On the contrary, the monoclinic-to-tetragonal phase transformation observed in nanosized zirconia irradiated by low-energy ion beams might be attributed to oxygen vacancy accumulation induced by displacement damage upon ballistic interactions.

The plausible mechanism of oxygen vacancies accumulation in controlling ZrO_2 monoclinic-to-tetragonal phase transformation is based on the importance of oxygen vacancies in stabilizing cubic and tetragonal ZrO_2 upon substitution of trivalent or divalent cations at Zr-sites. Previous literatures also suggested the significance of oxygen vacancies in the stabilization of tetragonal ZrO_2. For example, Kountouros et al.[29] has experimentally

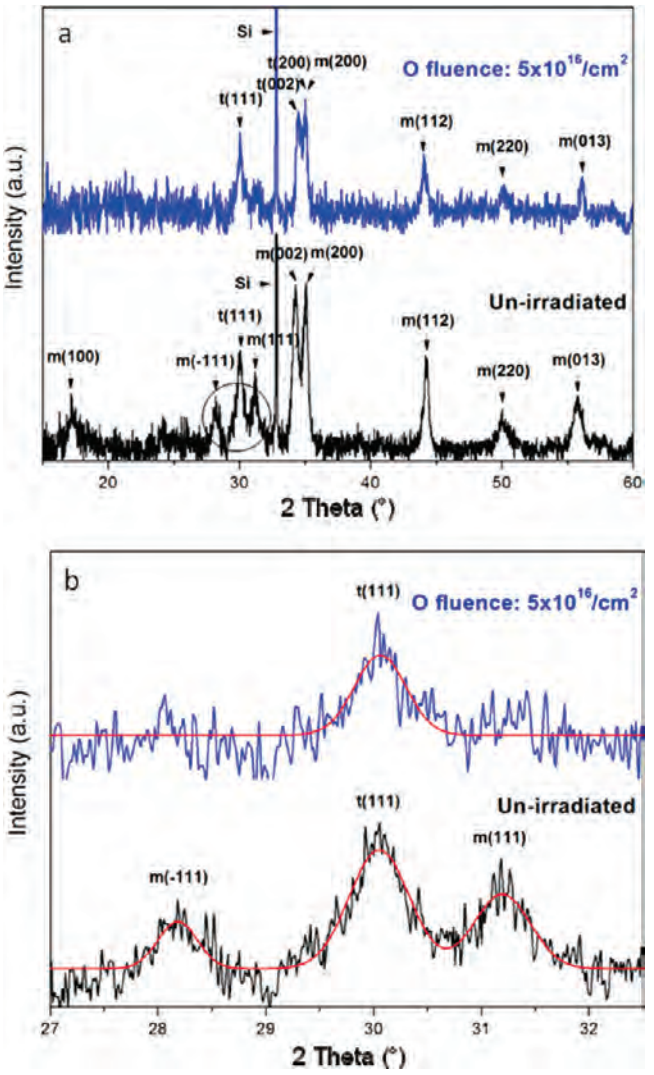

Figure 10. (a) XRD results of 1000 °C annealed ZrO_2 thin films before and after 350 keV O^+ irradiation at a fluence of $5 \times 10^{16}/cm^2$ (~3.3 dpa), (b) close-up XRD patterns within the 2θ range of 27−32.5° showing the characteristics of tetragonal and monoclinic phases.

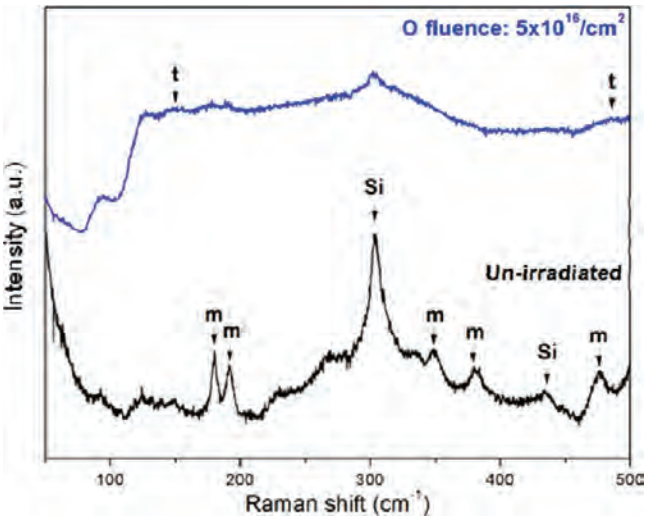

Figure 11. Raman spectra of 1000 °C annealed ZrO_2 thin films before and after 350 KeV O^+ irradiation at a fluence of $5 \times 10^{16}/cm^2$ (~3.3 dpa).

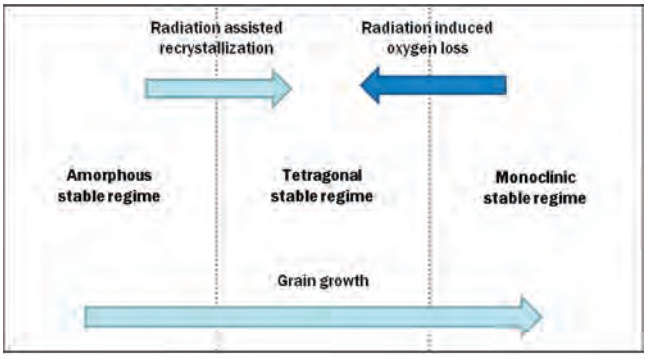

Figure 12. ZrO_2 phase stability at equilibrium (indicated by the lower grain growth arrow) and under the nonequilibrium radiation conditions (indicated by the two upper arrows). Possible mechanisms are included for irradiation-induced phase transformation in nanocrystalline zirconia.

demonstrated that by controlling the oxygen vacancy concentration through cation doping, ZrO_2 tetragonal phase can be stabilized at room temperature, and monoclinic-to-tetragonal and tetragonal-to-cubic phase transformations can be achieved by increasing the oxygen vacancy concentration. Such correlation between oxygen vacancy and the stabilization of tetragonal zirconia has also been demonstrated in several other studies.[30−32]

Upon energetic Kr^{2+} or O^+ beam irradiations, Frenkel defects (vacancies and interstitials of cation and anions) are created in nanocrystalline ZrO_2, and the high density of grain boundaries may provide effective channels for defect migration and diffusion, specifically for oxygen interstitials that may display a larger diffusion coefficient in ZrO_2 than vacancies.[33] As a result, oxygen interstitials may be annihilated at the grain boundaries or surfaces of nanocrystalline ZrO_2 grains if the grain size is comparable to the characteristic diffusion length or may even diffuse out along the grain boundaries leading to oxygen vacancy accumulation inside the grains and oxygen loss from the ZrO_2 matrix. The gradual accumulation of oxygen vacancies inside ZrO_2 grains above a critical value of vacancy concentration with increasing ion fluence may lead to a phase transformation from monoclinic to tetragonal. The mechanism is further testified by a recent study in which energetic beam bombardment can lead to oxygen loss in nanosized cubic ZrO_2.[34] Other possible mechanisms for driving this phase transformation may include the cascade overlap or direct impact, in which the temperature inside cascade cores upon the irradiation within picosecond time frame can exceed the monoclinic-to-tetragonal phase transition temperature of ZrO_2, leading to the formation of tetragonal domains. Upon the cascade quench, the tetragonal domains can be stabilized and the accumulation of these domains may eventually lead to the monoclinic-to-tetragonal phase transformation.

It is worth noting that, even though amorphous-to-tetragonal and monoclinic-to-tetragonal phase transformations are two processes thermodynamically different, they converge at tetragonal phase in the nonequilibrium states under intensive radiation conditions. Evidently, tetragonal ZrO_2 can be kinetically stabilized under intense radiation conditions for both bulk and nanosized regimes as the beam bombardment may provide

enough energy to overcome the barrier among different polymorphs. The ion irradiation stabilized tetragonal ZrO_2 phase coincides the thermodynamics in which metastable tetragonal phase is more energetically favorable at nanosized regimes due to a crossover in total energy. These results highlight an elegant example that the thermodynamic understanding might help to predict materials behavior under extreme conditions. In addition to temperature, pressure, grain-size, and chemical stabilizers, the nonequilibrium radiation condition adds another dimension to the control of phase stability of ZrO_2 polymorphs with different mechanisms as compared with that of the grain-size controlled stability under equilibrium condition (illustrated in Figure 12).

4. CONCLUSIONS

In conclusion, we identify a two-step amorphous-to-tetragonal and tetragonal-to-monoclinic phase transformation sequence in nanosized ZrO_2 induced by thermal annealing from 500 to 1000 °C, accompanied by a significant grain growth from ~5 to ~50 nm. The phase transformation processes upon thermal annealing are closely correlated to the grain-size controlled phase stability as a result of total energy crossover at different size regimes for nanosized zirconia, suggesting a comparable effect of temperature and grain size. Under energetic ion beam irradiation, a thermodynamically metastable tetragonal phase can be stabilized and both amorphous-to-tetragonal and monoclinic-to-tetragonal phase transformations can be achieved with different mechanisms. The amorphous-to-tetragonal phase transformation might be induced by radiation-induced recrystallization processes, whereas the monoclinic-to-tetragonal phase transformation might be the result of oxygen vacancy accumulation upon intensive ballistic interaction. Of particular importance, the thermodynamically stable monoclinic phase can be greatly suppressed and the favorable tetragonal phases with enhanced thermo-mechanical properties can be achieved at room temperature using ion beam techniques. By controlling beam conditions (ion fluences, energy, electronic energy loss, annealing temperature), we are able to tailor materials phase stability, grain size, and corresponding tetragonality for various engineering applications.

AUTHOR INFORMATION

Corresponding Author

*E-mail: lianj@rpi.edu. Telephone: 1-518-276-6081. Fax: 518-276-6025.

ACKNOWLEDGMENT

This work was supported as part of the Materials Science of Actinides, an Energy Frontier Research Center, funded by the Office of Basic Energy Sciences under Award Number DE-SC0001089. The deposition of zirconia thin film on Si substrates by IBAD approach was supported by the Nebraska Research Initiative and the University of Nebraska Medical Center. We thank the staff of the IVEM-tandem Facility at the Argonne National Laboratory for their assistance during ion irradiation and in situ TEM observation. The authors also acknowledge the insight discussion with Prof. Alexandra Navrotsky at University of California, Davis, in understanding the thermodynamics and kinetics of the phase transformation among different nanosized zirconia polymorph. F.Y. Lu is partially supported by NSF DMR 0906349 and Nuclear Regulatory Commission under an award number of NRC-38-09-954.

REFERENCES

(1) Clinard, F. W.; Rohr, D. L.; Ranken, W. *J. Am. Ceram. Soc.* **1977**, *60*, 287–288.
(2) Vance, E. R.; Boland, J. N. *Rad. Effects* **1978**, *37*, 237–239.
(3) Degueldre, C.; Kasemeyer, U.; Botta, F.; Ledergerber, G. *Mater. Res. Soc. Symp. Proc.* **1996**, *412*, 15–23.
(4) Oversby, V. M.; McPheeters, C. C.; Degueldre, C.; Paratte, J. M. *J. Nucl. Mater.* **1997**, *245*, 17–26.
(5) Burakov, B. E.; Anderson, E. B.; Galkin, B. Y.; Starchenko, V. A.; Vasiliev, V. G.; edited by Merz, E. R.; Walter, C. E. *Disposal of Weapon Plutonium - Approaches and Prospects*: Kluwer Academic: Dordrecht, The Netherlands, 1996; p 85.
(6) Moon, J.; Choi, H.; Kim, H.; Lee, C. *Surf. Coat. Technol.* **2002**, *155*, 1–10.
(7) Trice, R. W.; Su, Y. J.; Mawdsley, J. R.; Faber, K. T.; De Arellano-Lopez, A. R.; Wang, H.; Porter, W. D. *J. Mater. Sci.* **2002**, *37*, 2359–2365.
(8) Kudoh, Y.; Takeda, H.; Arashi, H. *Phys. Chem. Miner.* **1986**, *13*, 233–237.
(9) Bouvier, P.; Djurado, E.; Lucazeau, G.; Le Bihan, T. *Phys. Rev. B* **2000**, *62*, 8731–8737.
(10) Wittels, M. C.; Sherrill, F. A. *J. Appl. Phys.* **1956**, *27*, 643–644.
(11) Sickafus, K. E.; Matzke, H.; Hartmann, T.; Yasuda, K.; Valdez, J. A.; Chodak, P.; Nastasi, M.; Verrall, R. A. *J. Nucl. Mater.* **1999**, *274*, 66–77.
(12) Meldrum, A.; Boatner, L. A.; Ewing, R. C. *Nucl. Instrum. Methods Phys. Res., Sect. B* **2003**, *207*, 28–35.
(13) Lian, J.; Zhang, J. M.; Namavar, F.; Zhang, Y. W.; Lu, F. Y.; Haider, H.; Garvin, K.; Weber, W. J.; Ewing, R. C. *Nanotechnology* **2009**, *20*, 245303.
(14) Namavar, F.; Cheung, C. L.; Sabirianov, R. F.; Mei, W. N.; Zeng, X. C.; Wang, G.; Haider, H.; Garvin, K. L. *Nano Lett.* **2008**, *8*, 988–996.
(15) Mondal, P.; Klein, A.; Jaegermann, W.; Hahn, H. *Solid State Ionics* **1999**, *118*, 331–339.
(16) Nitsche, R.; Winterer, M.; Hahn, H. *Nanostructured Mater.* **1995**, *6*, 679–682.
(17) Djurado, E.; Bouvier, P.; Lucazeau, G. *J. Solid State Chem.* **2000**, *149*, 399–407.
(18) Chen, H.; Ding, C. X. *Surf. Coat. Technol.* **2002**, *150*, 31–36.
(19) Gulino, A.; LaDelfa, S.; Fragala, I.; Egdell, R. G. *Chem. Mater.* **1996**, *8*, 1287–1291.
(20) Boobalan, K.; Vijayaraghavan, R.; Chidambaram, K.; Mudali, U. M. K.; Raj, B. *J. Am. Ceram. Soc.* **2010**, *93*, 3651–3656.
(21) Ishigame, M.; Sakurai, T. *J. Am. Ceram. Soc.* **1977**, *60*, 367–369.
(22) Keramida, V. G.; White, W. B. *J. Am. Ceram. Soc.* **1974**, *57*, 22–24.
(23) Clearfield, A. *Inorg. Chem.* **1964**, *3*, 146–148.
(24) Garvie, R. C. *J. Phys. Chem.* **1965**, *69*, 1238–1243.
(25) Pitcher, M. W.; Ushakov, S. V.; Navrotsky, A.; Woodfield, B. F.; Li, G. S.; Boerio-Goates, J.; Tissue, B. M. *J. Am. Ceram. Soc.* **2005**, *88*, 160–167.
(26) Namavar, F.; Wang, G.; Cheung, C. L.; Sabirianov, R. F.; Zeng, X. C.; Mei, W. N.; Bai, J.; Brewer, J. R.; Haider, H.; Garvin, K. L. *Nanotechnology* **2007**, *18*, 415702.
(27) Benyagoub, A.; Levesque, F.; Couvreur, F.; Gibert-Mougel, C.; Dufour, C.; Paumier, E. *Appl. Phys. Lett.* **2000**, *77*, 3197–3199.
(28) Valdez, J. A.; Chi, Z. H.; Sickafus, K. E. *J. Nucl. Mater.* **2008**, *381*, 259–266.
(29) Kountouros, P.; Petzow, G. in: Badwal, S. P. S.; Bannister, M. J.; Hannink, R. H. J. (Eds.) *Science and Technology of Zirconia V*: Technomic: Lancaster & Basel, 1993; pp 30—48.
(30) Eichler, A. *Phys. Rev. B* **2001**, *64*, 174103.
(31) Guo, X. *Solid State Ionics* **1998**, *112*, 113–116.

(32) Lu, X. Y.; Liang, K. M.; Gu, S. R.; Zheng, Y. K.; Fang, H. S. *J. Mater. Sci.* **1997**, *32*, 6653–6656.
(33) Keneshea, F. J.; Douglass, D. L. *Oxid. Met.* **1971**, *3*, 1–14.
(34) Zhang, Y. W.; Jiang, W. L.; Wang, C. M.; Namavar, F.; Edmondson, P. D.; Zhu, Z. H.; Gao, F.; Lian, J.; Weber, W. J. *Phys. Rev. B* **2010**, *82*, 184105.